ORIGINAL PAPER

Microneedle-based nanoporous gold electrochemical sensor for real-time catecholamine detection

Cristina Tortolini[1] · Anthony E. G. Cass[2] · Riccardo Pofi[3] · Andrea Lenzi[3] · Riccarda Antiochia[1]

Abstract

Dopamine (DA), epinephrine (EP), and norepinephrine (NEP) are the main catecholamine of clinical interest, as they play crucial roles in the regulation of nervous and cardiovascular systems and are involved in some brain behaviors, such as stress, panic, anxiety, and depression. Therefore, there is an urgent need for a reliable sensing device able to provide their continuous monitoring in a minimally invasive manner. In this work, the first highly nanoporous gold (h-nPG) microneedle-based sensor is presented for continuous monitoring of catecholamine in interstitial fluid (ISF). The h-nPG microneedle-based gold electrode was prepared by a simple electrochemical self-templating method that involves two steps, gold electrodeposition and hydrogen bubbling at the electrode surface, realized by sweeping the potential between $+0.8$ V and 0 V vs Ag/AgCl for 25 scans in a 10 mM $HAuCl_4$ solution containing 2.5 M NH_4Cl, and successively applying a fixed potential of -2 V vs Ag/AgCl for 60 s. The resulting microneedle-based h-nPG sensor displays an interference-free total catecholamine detection expressed as NEP concentration, with a very low LOD of 100 nM, excellent sensitivity and stability, and fast response time (<4 s). The performance of the h-nPG microneedle array sensor was successively assessed in artificial ISF and in a hydrogel skin model at typical physiological concentrations.

Keywords Microneedles · Nanoporous gold needle · Electrochemical sensor · Catecholamine · Dopamine · Epinephrine · Norepinephrine

Introduction

Catecholamines (CAs) are monoamine compounds of the central and peripheral nervous system [1], which act as both neurotransmitters (NTs) and hormones. They include dopamine (DA), norepinephrine (NEP; also called noradrenaline (NA)), and epinephrine (EP; also called adrenaline (Adr)). They share the same catechol moiety, hence their name, and the same amino acidic precursor tyrosine. In resting individuals, endogenous CA concentrations in blood and interstitial fluid are approximately 150–800 ng/L for NEP and 10–50 ng/L for both NEP and DA [2]. The link between

these amine compounds and human pathologies has been known for over 100 years [3]. Neurological disorders, such as Alzheimer and Parkinson's diseases, the two most common neurodegenerative disorders; schizophrenia; and hyperactivity, are some examples of neurologic and psychiatric disorders related to catecholamine levels in the human body [3]. Normally, catecholamines and their metabolites are present in the body in small, fluctuating amounts, that only increase appreciably during and shortly after a stressful situation [4]. However, rare tumors called pheochromocytomas and neuroblastomas can produce large amounts of these hormones, resulting in increased concentrations in both blood and urine [5]. Therefore, there is a great need for a reliable sensing device to monitor catecholamine concentrations in biofluids, as they represent clinically relevant biomarkers for a particular disease or to monitor treatment efficacy. Moreover, the continuous real-time detection of CAs in both in vitro and in vivo experiments result of upmost importance in biomedical research to investigate the physiological role of these compounds in neurotransmissions events associated with various diseases or reward-related behaviors.

✉ Riccarda Antiochia
riccarda.antiochia@uniroma1.it

1 Department of Chemistry and Drug Technologies, Sapienza University of Rome, P.le Aldo Moro 5, 00185 Rome, Italy

2 Department of Chemistry & Institute of Biomedical Engineering, Imperial College, London, UK

3 Department of Experimental Medicine, Sapienza University of Rome, Rome, Italy

Considering that CAs have a very short half-live and are often secreted in an episodic manner, their levels might appear normal between secretory phases [6], creating a diagnostic problem. The opportunity for new methods, continuous monitoring, and real-time detection of CAs could overcome such issues, and offer a dramatic improvement in the diagnosis and follow-up management of diseases characterized by CA excess such as phaeochromocytomas and paragangliomas.

Numerous analytical methods have been developed including HPLC [7], UV spectrophotometry [8], mass spectroscopy [9], chemiluminescence [10], and electrochemical (EC) methods [2, 11]. In particular, EC methods have attracted a lot of attention, thanks to their favorable properties, such as simplicity, fast response time, high sensitivity, cost effectiveness, suitability for multiple detection, and possibility of miniaturization [2]. These features allow to overcome the most common drawbacks of the other techniques, such as time consuming and expensive laboratory equipment and trained personnel.

Electrochemical sensors and biosensors proved to be highly sensitive and selective techniques in the determination of CAs in biological fluids, while remaining inexpensive [2].

A critical problem associated with the detection of CAs is the coexistence of interfering compounds within the biological samples. The most important interfering compounds are ascorbic acid (AA) and uric acid (UA). They show similar oxidation potentials at conventional bare electrodes showing overlapping voltammetric signals, thus preventing a proper separation [12].

Another problem associated with the electrochemical detection of CAs is the so-called "biofouling process," which is a passivation of the electrode surface, due the polymerization of the oxidation products of CAs [13].

To minimize interfering signals and to avoid surface passivation, several sensor surface modification approaches were undertaken. Initially, two strategies were adopted: covering of the electrode surface with conducting polymers [14, 15] and the formation of SAMs on oxide-free metals, especially gold surface. Unfortunately, the sensors based on these approaches require pre-concentration of CAs before measurements, with limited clinical application [2]. More recently, the coupling of nanotechnology with sensors/biosensors allowed the development of excellent models for both in vivo and in vitro quantitative analysis of CAs at physiological levels [15]. Metal nanoparticles [16], carbon nanotubes [17], and graphene [18] are the most used nanomaterials in the development of the new-generation EC sensors with enhanced performances, thanks to their high surface area, high electrocatalytic activity, improved selectivity, and fast mass transport [2]. Very recently, two-dimensional (2D) materials, such as transition metal dichalcogenides (TMDs), thanks to their tunable electronic/optical properties, are emerging as a new material platform to develop

ultrasensitive sensors for CA detection [19]. Nanoporous metals [20, 21] have been also studied as sensitive electrodes thanks to their large surface area/volume ratio. In particular, nanoporous gold (nPG) has recently reached increasing attention because of its unique properties of high electrical conductivity, electrocatalytic activity, selectivity, and antifouling capacity [22–24].

However, most of the nano-based sensors allowed the determination of CAs either in plasma, with discomfort of the patient of having blood drawn; moreover usually blood needs to be taken after 30 min of supine rest with an indwelling catheter and, ideally, in the fasting state [25], or in 24-h urine samples [26].

Recent studies are investigating the possibility to measure CA concentrations in minimally invasive and more practical biofluids, such as sweat, thus allowing also a continuous monitoring with the development of wearable devices. At present, only two sensor platforms for the detection of DA in sweat have been reported, but unfortunately the detection limit is slightly higher than that obtained in plasma and urine [19, 27]. Moreover, these sensors cannot be as accurate as blood and urine tests because the content of sweat is more variable, being influenced by several factors.

Another interesting biological fluid for wearable sensors is the ISF, the fluid which surrounds the body cells, providing nutrients that directly diffuse from the capillary endothelium. Hence, many analytes, used in current clinical practice, are common to ISF and blood plasma, showing a reliable correlation with comparable concentration values [28] thanks to the equilibrium between the two fluids. Over the past three decades, researchers have utilized the ISF for non-invasive detection of metabolic diseases, organ failure, and drug efficacy, using the microneedle technology for ISF extraction and sensing [29]. More recently, the microneedle array technology is used for the assembling of wearable electrochemical sensors and biosensors [30]. Microneedle array-based sensors allow minimally invasive and continuous monitoring of important clinical biomarkers in ISF [28]. The method is well tolerated by patients, as the microneedles penetrate the stratum corneum at less than 1-mm depth, without reaching deep in the lower part of dermal compartment, where nerve and blood vessels are mainly present [31–34]. Moreover, microneedle-based devices have the advantage to accommodate multiple sensors on the same array, to provide multiplexed analysis.

In this work, we describe the first example of a microneedle-based highly nanoporous gold (h-nPG) electrochemical sensor for selective and continuous monitoring of total CAs in ISF. The gold surface of the microneedles has been modified in a simple and scalable way, by a "self-templating" electrodeposition procedure of a h-nPG film, as shown in Scheme 1. The morphology was characterized through scanning electron microscopy (SEM) and electrochemical
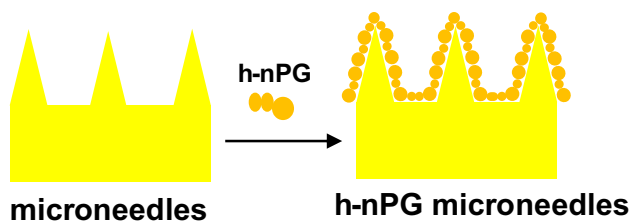
Scheme 1 Schematic representation of the h-nPG-modified microneedle electrode

impedance spectroscopy (EIS). The microneedle-based h-nPG electrode showed significant selectivity for the detection of DA, NEP, and EP in presence of higher concentrations of ascorbic acid (AA) and uric acid (UA) and other interferents. The interesting analytical performances of the sensor were tested in artificial ISF and in a hydrogel skin model, showing promising results.

Experimental

Chemicals and reagents

Dopamine hydrochloride (DA), epinephrine bitartrate salt (EP), norepinephrine bitartrate salt monohydrate (NEP), sodium monobasic phosphate (Na_2HPO_4), sodium dibasic phosphate (NaH_2PO_4), potassium chloride (KCl), potassium ferricyanide (III) ($K_3[Fe(CN)_6]$), potassium ferrocyanide (II) ($K_4[Fe(CN)_6]$), gold (III) chloride solution, and ammonium chloride (NH_4Cl) were purchased from Sigma-Aldrich (Buchs, Switzerland). All solutions were prepared in phosphate buffer 0.1 M, KCl 0.1 M, pH 7.4 (PBS). High-purity deionized water (resistance: 18.2 MΩ cm at 25 °C; TOC < 10 μg L^{-1}) obtained from Millipore (Molsheim, France) has been used throughout experiments.

Preparation of artificial interstitial fluid (ISF) and hydrogel skin model

The artificial interstitial fluid (ISF) was prepared by mixing 2.5 mM$CaCl_2$, 5.5 mM glucose, 10 mM HEPES, 3.5 mM KCl, 0.7 mM $MgSO_4$, 123 mM NaCl, 1.5 mM NaH_2PO_4, and 7.4 mM saccharose. The pH was adjusted to pH 7.4 [35]. The hydrogel skin model was prepared by dissolving 200 mg of agarose in 10 mL of 0.1 M PBS pH 7.4 and stirred at 120 °C in a glass until complete dissolution. Successively, the liquid is poured in a Petri dish (35 mm in diameter) containing 2.0 mL of artificial ISF and allowed to solidify. Finally, solutions containing proper NEP concentrations were drop-casted onto the Petri dish in order to have final NEP concentrations of 0, 5, 10, 20, 30, 50, 60, 75, 100, 185,

450, and 850 μM and allowed to diffuse for 1 h through the gel [34].

Electrode preparation and modification

The microneedle-based h-nPG electrodes were modified by an self-templating electrodeposition method consisting of two steps: (i) sweeping the potential for 25 scans between + 0.8 V and 0 V vs Ag/AgCl at 50 mV s^{-1} in a 10 mM $HAuCl_4$ solution containing 2.5 M NH_4Cl and (ii) applying a fixed potential of − 2 V vs Ag/AgCl to the modified electrode for 60 s in the same solution, in order to allow the formation of pores, due to hydrogen bubbling. The H_2 bubbles are generated in situ in a solution containing H^+ (self-templating procedure, without the use of an external template). Finally, the electrodes were further activated in 0.5 M H_2SO_4, by running CVs between 0 and + 1.7 V vs Ag/AgCl at a scan rate of 100 mV s^{-1} for 25 cycles, until a well-defined CV was obtained [36].

SEM experiments

Scanning electron microscopy (SEM) measurements were carried out with a High-Resolution Field Emission Scanning Electron Microscopy (SEM) (HR FESEM; Zeiss Auriga Microscopy, Jena, Germany), in order to investigate the morphology of the bare and modified screen-printed electrodes (SPEs).

Energy-dispersive X-ray spectroscopy (XPS) measurements were performed in order to evaluate the Au content of the h-nPG-modified screen-printed electrode. The EDX spectrum and data were collected during sample surface scanning by SEM electron probe.

Electrochemical measurements

All electrochemical measurements were performed in a 10-mL thermostated glass cell (model 6.1415.150, Metrohm (Herisau, Switzerland)) with a conventional three-electrode configuration with an Ag/AgCl/KCl$_{sat}$ (198 mV vs NHE) as reference electrode (cat. 6.0726.100, Metrohm, Herisau, Switzerland), a glassy carbon rod as a counter electrode (cat. 132 6.1248.040, Metrohm, Herisau, Switzerland), and a gold classical electrode (diameter 2 mm) as working electrode (Au, cat. 6.1204.320, Metrohm, Herisau, Switzerland). A gold screen-printed electrode (Au-SPE, 220BT Metrohm, Herisau, Switzerland, Aux: gold; Ref: silver, diameter 4 mm) was also used as working electrode.

The microneedle-array Au microneedle electrodes were fabricated at Glasgow University [32] and metallized by Torr Scientific Ltd. (Bexhill). They are based on a polycarbonate scaffold (0.5 × 0.5 × 0.02 cm) with 64 microneedles divided as four 4 × 4 arrays. Each pyramid showed the

following dimensions: base 0.06 cm, height 0.1 cm, and 4×4 array area 0.2 cm^2. On this platform, three electrodes were used as working electrodes (gold), while the fourth one was the reference electrode (silver). In our work, we used the gold array as working electrode and external Ag/AgCl/KCl$_{sat}$ and glassy carbon rod (described above) as reference and counter electrode, respectively.

EIS experiments were carried out at equilibrium potential called open-circuit potential (OCP) without potential of the redox probe (0.22 V vs Ag/AgCl), bias voltage in the frequency range of $0.1–10^3$ Hz using an AC signal of 10-mV amplitude at a formal potential of the redox probe (0.22 V vs Ag/AgCl), using Autolab Potentiostat/Galvanostat (Eco Chemie, Netherlands). EIS measurements were performed using 10 mL of PBS solution containing mixture of 5 mM $Fe(CN)_6^{3-}$/$Fe(CN)_6^{4-}$, as electrochemical probe.

Results and discussion

SEM characterization and microanalysis of h-nPG microneedle electrodes

The morphology and components of the microneedles were characterized by SEM and SEM–EDX experiments, respectively. SEM images were used to investigate the physical appearance and the surface characteristics of the microneedle-based electrode before and after the electrodeposition of the h-nPG film. Figure 1 shows the SEM images of the bare (panels A and B) and the h-nPG microneedle-based electrodes (panels C and D), at different magnifications. It is possible to note that a h-nPG film is deposited onto the microneedle-based electrode surface after the electrodeposition method, exhibiting evenly distributed nanopores with diameter of a few nanometers (panel C), typical of a sponge-like structure (panel D).
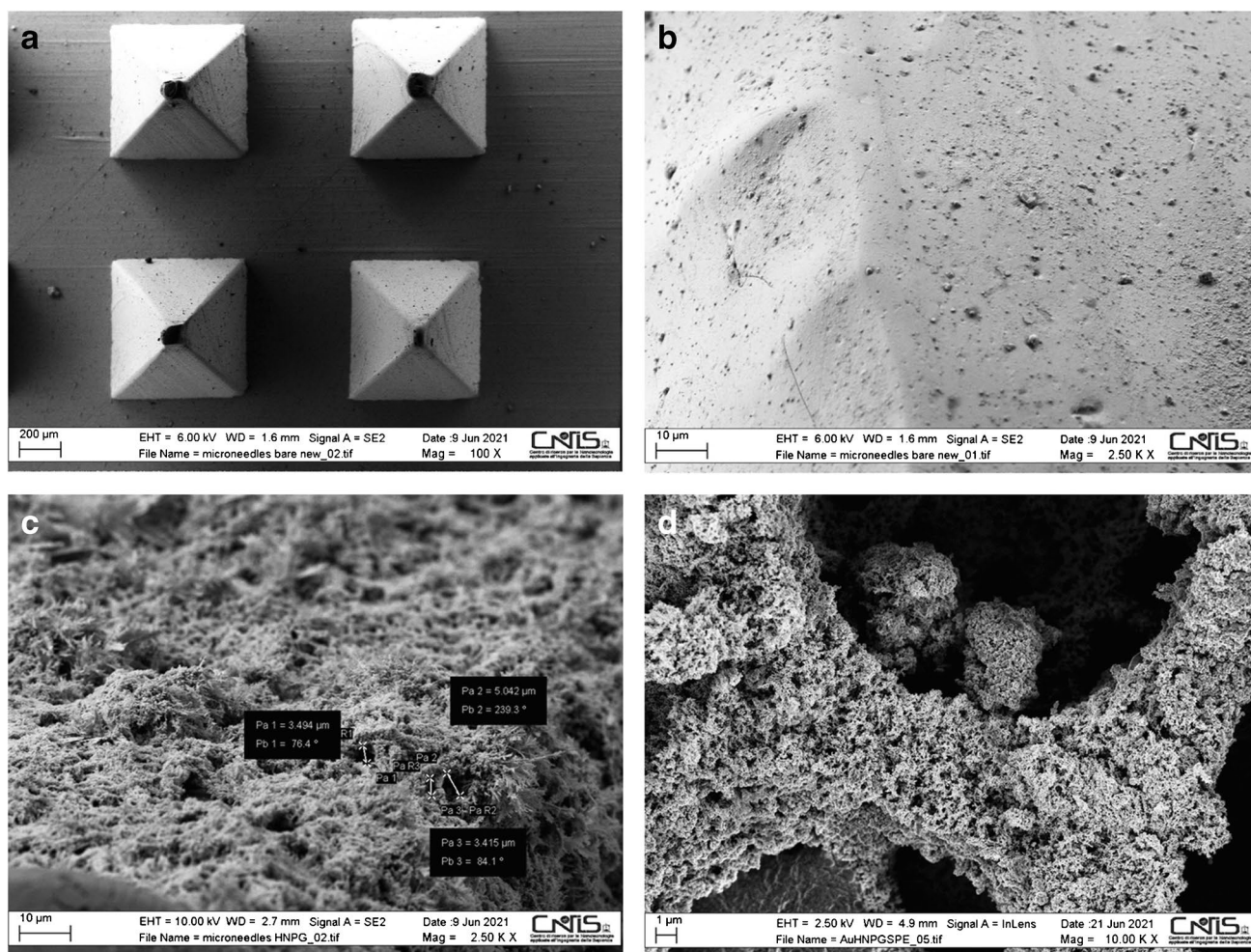

Fig. 1 SEM images of Au bare microneedles (**A** and **B**) and h-nPG microneedle electrode (**C** and **D**)

The EDX microanalysis was carried out in order to exclude any potential contaminant in the electrodeposited film. The EDX spectrum and the content percentage of each element are shown in Fig. S1, panels A and B. The spectrum clearly indicates that the product is mainly composed of Au with traces of C, O, and N. It depicts a strong band at 2.15 keV, which is the typical optical adsorption of gold nanocrystals. The high- and low-intensity bands at 0.25 and 9.71 keV also correspond to Au, in accordance with the EDX energy table. It is interesting to note the absence of chloride as possible contaminant, although the electrodeposited film is generated from a gold chloride solution.

Electrochemical behavior of h-nPG microneedle electrodes

The electrochemical behavior of the h-nPG microneedle electrodes was monitored by cyclic voltammetry (CV) and electrochemical impedance spectroscopy (EIS) experiments.

CV characterization

The electrochemical characterization of the microneedle electrode before and after h-nPG electrodeposition has already been investigated by CV in a solution of $Fe(CN)_6^{3-}/^{4-}$, as reported in our previous work [36]. It is interesting to note that the enhancement of both anodic and cathodic peak current densities after the h-nPG electrodeposition was much larger than that registered with planar gold electrodes after the same modification. The increase of the electroactive surface area after the formation of the h-nPG film obviously occurs in both cases, but the particular geometry of the microneedles seems to play an important role, allowing a better electrodeposition of the h-nPG film and therefore achieving a larger electroactive surface area [36].

EIS characterization

EIS was carried out to investigate the impedance alteration at the electrode-solution interface after the h-nPG modification of the microneedle-based gold electrode. It is known that the Nyquist plot consists of a semicircular part and a linear part. At high frequencies, the semicircle part corresponds to the electron transfer resistance (R_{ct}), measured as the semicircle diameter, which gives information about the electron transfer kinetics on the electrode surface. At low frequencies, the linear part is indicative of systems under diffusion-controlled current [37]. Figure 2 (panels A–C) are the Nyquist plot of unmodified Au (A) and microneedle Au electrodes before (B) and after (C) the modification with the h-nPG film. It is possible to observe a clear reduction of the semi-circular part when the microneedle-based electrode is used compared to Au bare electrode. This can be

ascribed to a better conductivity, probably obtained thanks to the particular geometry of the microneedles [36]. A further decrease of the charge-transfer resistance is observed with the h-nPG-modified microneedle electrode, indicating the good electrical conductivity of the nanoporous film, which promotes a higher electron transfer rate in the redox probe.

The EIS data were successively fitted, and the corresponding equivalent circuit is reported in Fig. 2, panel D. It is interesting to note, as reported in Fig. 2 panel E, that there is a drastic decrease of the R_{ct} value with h-nPG microneedle electrode ($1 \ 10^{-6}$ Ω), compared to Au bare microneedle electrode (125 Ω), suggesting that the nanoporous structure of the h-nPG film allows a higher electron transfer rate in the redox probe, thanks to the high conductivity of the nanostructures.
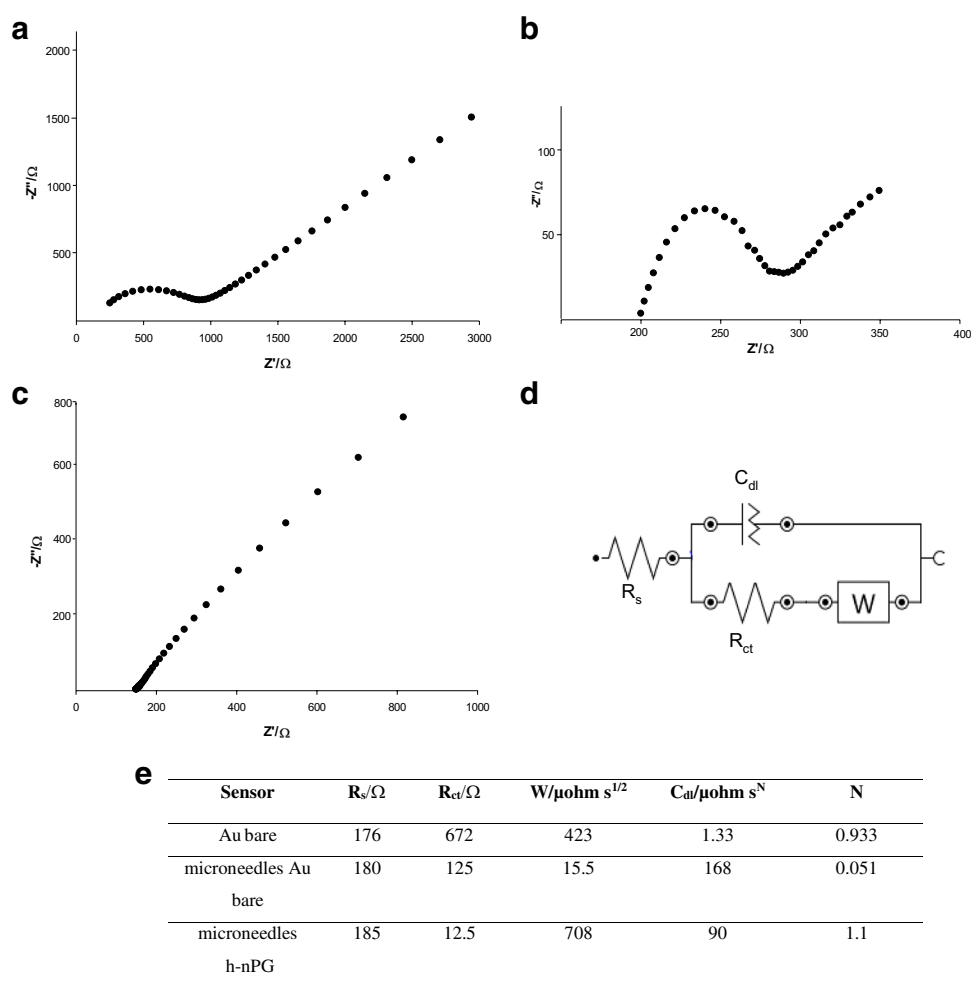
Electrocatalytic oxidation of DA, EP, and NEP at h-nPG microneedle electrode

The electrocatalytic behavior of DA, EP, and NEP at bare and modified microneedle electrode was investigated in PBS pH 7.4 containing 100 µM of each catecholamine, as shown in Fig. 3 (panels A, B, and C). It is clearly noted that microneedle-modified electrodes showed significantly higher DA, EP, and NEP oxidation currents (1000-fold) and lower oxidation potentials, compared to bare microneedle electrodes. The large oxidation currents and low oxidation potential values shown by the h-nPG microneedle electrodes suggest the enhanced electrocatalytic behavior of the nanoporous film toward oxidation of each catecholamine, compared to bare microneedle electrodes. Moreover, the modified electrodes showed sharper and well-defined oxidation peaks compared to bare electrodes. This result might be due to the faster electron transfer rate at the modified electrode/solution interface, thanks to the increased electrical conducting surface area of the nanoporous film and the entrapment of the electroactive species inside the nanoporous, which allows negligible mass transfer and shorter diffusion times [38, 39].

CV of bare microneedle electrodes show a total electrochemically irreversible behavior towards detection of NEP, as no defined anodic and cathodic peak currents were observed (Fig. 3, inset panel C), and a quasi-reversible behavior in the case of DA and EP, with a potential peak separation (ΔE_p) of about 65 mV vs Ag/AgCl (Fig. 3, inset panels A,B).

The combined effect of the improved peak current responses and the low ΔE_p obtained with h-nPG microneedle electrode for DA, EP, and NEP must be due to the synergistic effect of the greater active surface area of the h-nPG film compared to bare electrode, as well as the faster electron transfer rate. The reversible behavior observed with all CAs after electrode modification provides clear evidence

Fig. 2 The Nyquist plots of bare Au electrode (**A**), microneedle bare Au electrode (**B**), and microneedle h-nPG electrode (**C**) in 5 mM $[Fe(CN)_6]^{3-/4-}$ + 0.1 M KCl and the equivalent circuit used for fitting the experimental data (**D**). (E) The EIS results from the electrochemical Nyquist plot fitting

Sensor	R_s/Ω	R_{ct}/Ω	$W/\mu ohm\ s^{1/2}$	$C_{dl}/\mu ohm\ s^N$	N
Au bare	176	672	423	1.33	0.933
microneedles Au bare	180	125	15.5	168	0.051
microneedles h-nPG	185	12.5	708	90	1.1

of the catalytic effect of the nanoporous film, which act as a promoter to enhance the electron transfer rate of the electrochemical reaction. The heterogeneous electron transfer rate constants ($k^0 cm\ s^{-1}$) for DA, EP, and NEP by h-NPG microneedle electrode have been calculated with a method proposed by Lavagnini et al. that merges the Klingler–Kochi and Nicholson and Shain methods developed for irreversible and reversible systems, respectively [40, 41] and resulted to be 3.5×10^{-3}, $4.0 \pm \times 10^{-3}$, and 4.2×10^{-3} cm s^{-1}, respectively.

It is reported in literature that the oxidation of DA, EP, and NEP occur via a complex two-electron two-proton transfer process, with parallel spontaneous side reactions leading to the formation of different oxidized species, which may inhibit the electron transfer, thus decreasing the electrode response sensitivity [42, 43]. The mechanism of the oxidation/reduction process of DA on the h-nPG electrode has been investigated by recording a cyclic voltammogram in a larger potential window, from −0.4 to 0.4 V vs Ag/AgCl. It is interesting to note that the h-nPG microneedle electrode shows one sharp oxidation peak in the positive scan from 0 to 0.4 V and two well-defined cathodic peaks at about 0.16

and −0.2 V vs Ag/AgCl in the reverse scan, as shown in Fig. S2 (panel A). The well-resolved cathodic peaks can be ascribed to the subsequent reduction of two oxidized species: dopaminequinone to dopamine and dopaminechrome, formed via a spontaneous intramolecular cyclization of dopaminequinone, to leucodopaminechrome, as schematized in Fig. 3, panel D [44]. In the potential range from −0.4 to 0 V a second small oxidation peak occurs, as a counterpart of the cathodic peak at −0.2 V, corresponding to the oxidation of leucodopaminechrome to dopaminechrome. Similar steps can be assumed for EP and NEP oxidation/reduction mechanisms (Fig. S2, panel B), due to the similarities of their reverse CV scans with DA (curves not shown).

Effect of scan rate

The scan rate effect on the anodic peak currents of DA, EP, and NEP was investigated at the developed nanoporous microneedle electrode at a fixed concentration (100 μM) of each catecholamine. CVs of DA at different scan rates (5–300 mV s^{-1}) have been registered and in Fig. 4 are reported between 5 and 50 mV s^{-1}. The anodic peak current
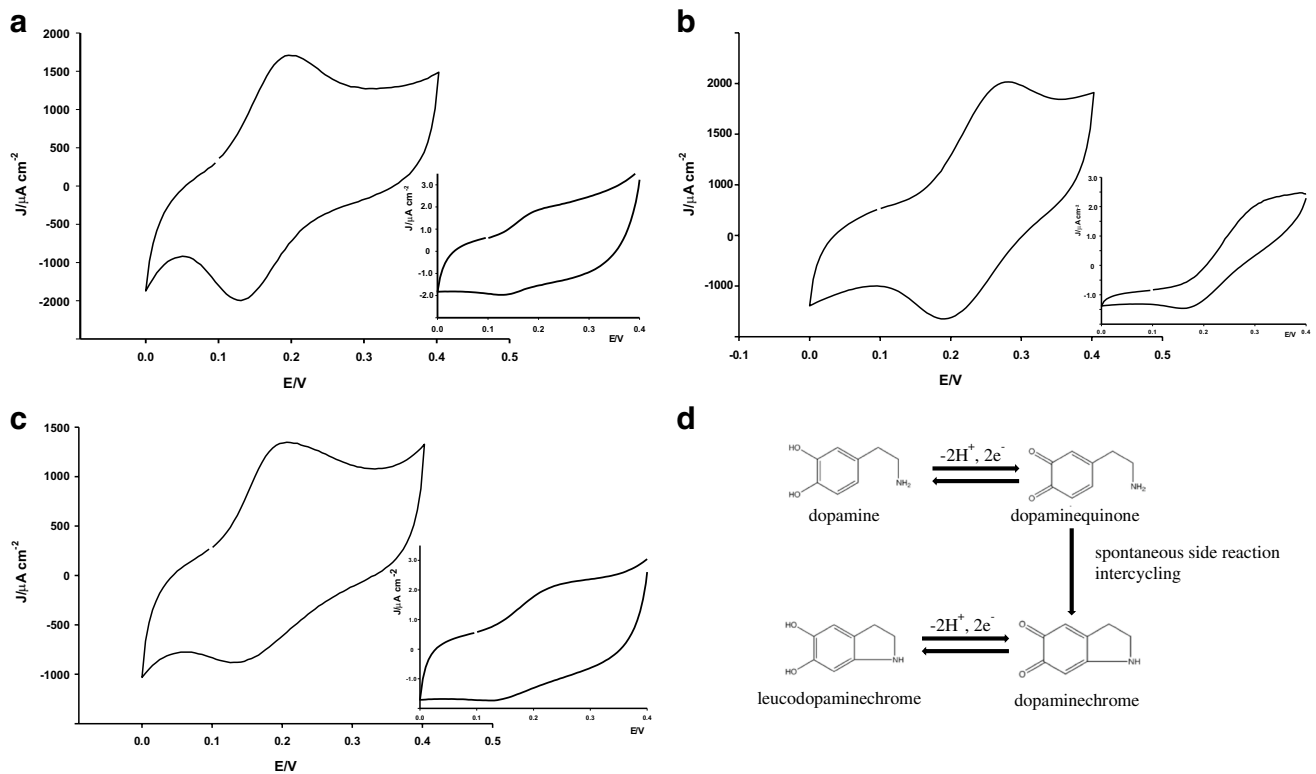
a

b

c

d

Fig. 3 CVs of 0.1 mM DA (**A**), EP (**B**), and NEP (**C**) in PBS 0.1 M, KCl 0.1 M, pH 7.4 at 25 mV s^{-1} using h-nPG microneedle electrode. In the insets Au bare microneedle electrode. (D) A possible DA oxidative pathway

Fig. 4 CVs of 0.1 mM DA, with microneedle h-nPG electrode at the following scan rates: 5 (black), 10 (red), 25 (blue), and 50 mV s^{-1} (pink) in 0.1 M PBS and 0.1 M KCl (pH 7.4). In the inset, the plot of the peak current density vs scan rate (5–300 mV s^{-1}) ($n=3$)
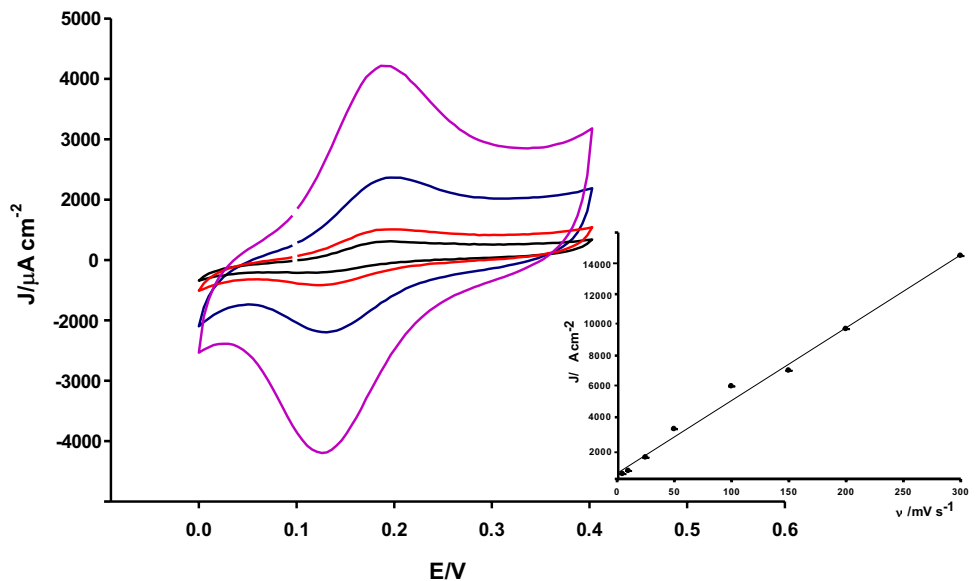
increases linearly with the scan rate with the following regression equation: J_{pa}/mA cm$^{-2}=0.04$ ν/mV s$^{-1}+1.9$ ($R=0.999$) (Table S1). The linear dependence of J_{pa} versus scan rate indicates a typical surface adsorption behavior (insets Fig. 4, panel A) [45], as already reported for different gold modified electrodes [46]. The adsorption of DA on the

surface of h-nPG electrode can be ascribed to a possible interaction between the amino group of DA and the nanoporous gold surface [47].

Different results were obtained for EP and NEP. The J_{pa} values of both EP and NEP resulted to be linear with ν at low scan rates, in the range 5–100 mV s^{-1}, suggesting a

surface-controlled process. At higher scan rates (between 150 and 300 mV s^{-1}), the plot of J_{pa} versus the square root of scan rate resulted to be linear, suggesting a diffusion rather than a surface-controlled process (Fig. S3, panels A and B). This particular trend may be attributed to a mixed diffusion-adsorption control of the redox process [38]. The linear regression equations of J_{pa} versus ν and $\nu^{1/2}$ for EP and NEP are reported in Table S1. It is interesting to note that this particular behavior is not obtained for EP and NEP with other nanocomposite-modified electrodes, showing a diffusion-controlled process [48]. Therefore, the surface phenomena reported for the developed nanoporous microneedle electrodes could be ascribed to their particular structure.

In addition, the charge transfer coefficient α and the standard heterogeneous rate constant (k_s) were calculated according to Laviron equation [45], by using the variation of the anodic and cathodic peak potentials versus logarithm of scan rate and the Laviron equation, respectively. At higher scan rates, the dependence of E_p versus log ν is linear (figure not shown) and the slopes of the linear part are -2.303 $RT/\alpha nF$ and 2.303 $RT/(1-\alpha)nF$ for cathodic and anodic peaks, respectively [45]. The charge transfer coefficients (α) calculated as the mean of the cathodic and anodic values resulted to be 0.69 for DA, 0.96 for EP, and 0.41 for NEP, respectively.

From the values of ΔE_p corresponding to different scan rates, average values of k_s were found to be 0.01, 0.002, and 0.003 s^{-1} for DA, EP, and NEP, respectively.

The surface coverages (Γ) of DA, EP, and NEP onto the microneedle-modified electrode were calculated from the plot of I_p versus scan rate ν, according to Eq. (1) [45]:

$$i_p = n^2 F^2 \nu A \Gamma / 4RT \tag{1}$$

where n is the number of electrons; F, R, and T are the Faraday constant, the molar gas constant, and the absolute temperature; ν is the scan rate; and Γ is the surface coverage. Assuming $n = 2$ for the three compounds, the Γ values of DA, EP, and NEP were found to be 5.35×10^{-8}, 0.06×10^{-8}, and 0.07×10^{-8} mol cm^{-2}, respectively. The data showed a similar order of magnitude compared to Γ values calculated for CAs with different electrode nanomodification reported in literature [46], indicating an increased adsorptivity of the h-nPG-nanomodified microneedle electrode.

The Tafel values were calculated by using Eq. (2), by plotting E_p versus log ν (Fig. S4):

$$E_p = (b/2)\log\nu + k \tag{2}$$

where E_p is the anodic peak potential (V), ν is the scan rate (mV s^{-1}), and b represents the Tafel value. The obtained values for the microneedle-modified electrode, in a 0.1 mM solution of each catecholamine, were 164, 74, and 80 mV dec^{-1} for DA, EP, and NEP, respectively. A high Tafel value

indicates a larger analyte adsorption. The Tafel values were found in the order DA > NEP > EP, confirming the larger adsorption of DA on the highly porous electrode surface.

The logarithm of the peak current (log i_p) vs logarithm of the scan rate (log ν) for DA, EP, and NEP is reported in Fig. S5. The slope values resulted to be 0.55, 0.20, and 0.36 for DA, EP, and NEP, respectively. It is known that a log ν value equal to 0.5 is typical of a diffusion-controlled process; a higher value is indicative of an adsorption process and a lower value of a mixed diffusion-adsorption process. Therefore, the results confirm that DA showed an adsorption-controlled process, on the contrary both EP and NEP a mixed diffusion-adsorbed process.

Apparent diffusion coefficients of DA, EP, and NEP at h-nPG microneedle electrode

The study of the dependence of the anodic peak currents against the scan rate was used for the estimation of the "apparent" diffusion coefficients D_{app} for DA, EP, and NEP at h-nPG microneedle electrodes. The D_{app} values were calculated from the slope of i_p vs $\nu^{1/2}$ plots, using the Randles–Sevcik equation:

$$i_p = 2.69 \times 10^5 n^{3/2} A C^0 D^{1/2} \nu^{1/2}$$

where i_p is the peak current density (A cm^{-2}), n is the number of electrons, A is the geometrical microelectrode area (cm^2), C_0 is the analyte concentration (5×10^{-6} mol cm^{-3}), ν is the scan rate, and D is the diffusion coefficient of the electroactive species (cm^2 s^{-1}).

The D_{app} value obtained for DA, EP, and NEP resulted to be 5.45×10^{-6}, 4.5×10^{-6}, and 7.3×10^{-6} cm^2 s^{-1}, respectively, consistent with values reported in literature [47].

Selectivity

Selectivity of the h-nPG microneedle electrode for DA, EP, and NEP was investigated separately by recording sensor responses in exposure to other potential interferents, such as AA and UA, which most frequently coexist in biological matrices. It is fundamental to selectively detect each single catecholamine in the presence of AA and UA, as they usually show overlapping voltammetric curves at both unmodified and chemically modified electrodes. Figure 5 shows the differential pulse voltammograms of ternary mixtures of a single catecholamine (DA, EP, or NEP) and AA and UA. It is possible to note three sharp, well-resolved anodic peaks at about 60, 200, and 360 mV for AA, each catecholamine and UA. Thus, the separations of the peaks were large enough to determine DA, EP, and NEP individually in the presence of a similar concentration of UA and a ten times higher concentration of AA.

Fig. 5 DPVs of 0.5 mM DA (**A**), EP (**B**), and NEP (**C**) 0.5 mM in presence of 4 mM AA and 0.6 mM UA with h-nPG microneedle electrode
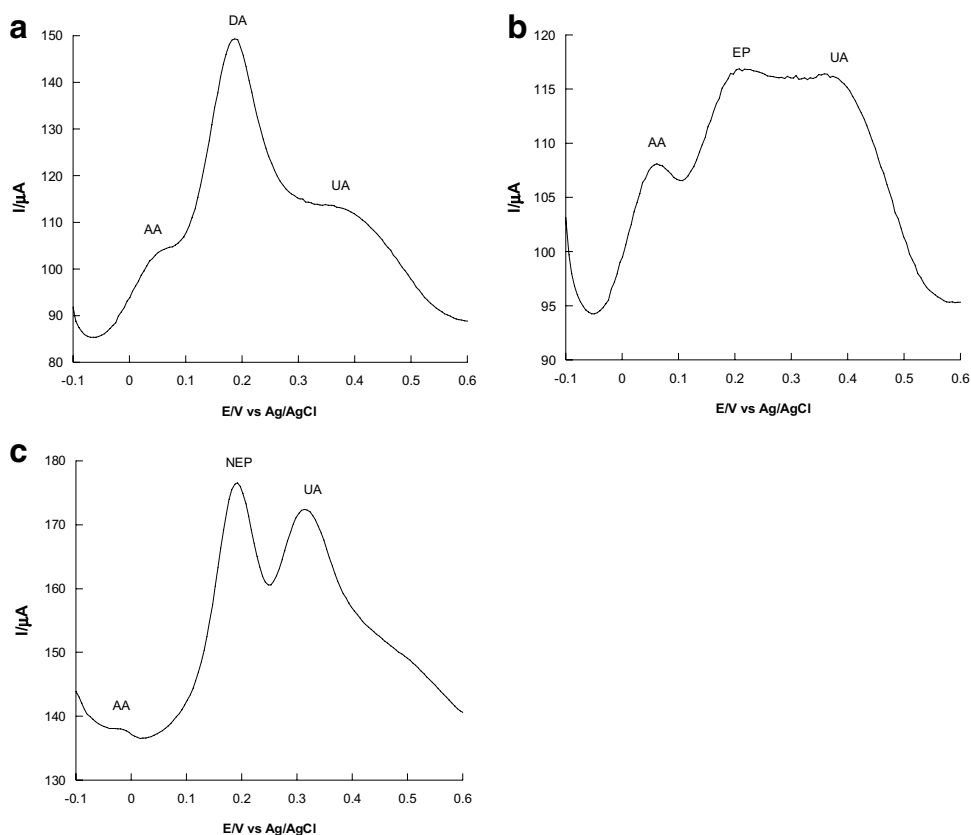
Successively, other possible interfering compounds have been tested by examining the DPV responses of 200 µM of DA, EP, and NEP in the presence of various interferents, such as L-cysteine, L-lysine, urea, citric acid, NaCl, and folic acid at 500 µM and glucose at 5 mM. The results are shown in Table 1. No significant influence was observed for all interfering compounds tested with maximum percentages of signal change of 4% for DA, 3% for EP, and 2% for NEP.

Reproducibility, repeatability, and stability

The reproducibility of the catecholamine sensors was evaluated using five independent h-nPG microneedle electrodes by measuring the peak currents of 10 µM of each catecholamine. The RSD of DA, EP, and NEP resulted to be 3.08%, 3.64%, and 2.24%, respectively, suggesting the excellent reproducibility of the sensors which attests that the h-nPG microneedle electrodes do not undergo significant surface biofouling during measurements.

In order to investigate the repeatability, the three sensors were used to perform 10 repetitive measurements in PBS containing 10 µM of each catecholamine. The RSD resulted to be 2.08%, 2.79%, and 1.99% for DA, EP, and NEP, respectively, showing remarkable repeatability.

The stability and lifetime of the sensors were investigated by testing the DPV responses of the three sensors for 10 measurements every day over a period of 30 days, for a 10 µM solution of each catecholamine, as reported in Fig. S6

Table 1 Influence of interfering compounds on DA, EP, and NEP response (200 µM) of the h-nPG microneedle sensor

Interfering compound	DA (µM)	Recovery (%)	EP (µM)	Recovery (%)	NEP (µM)	Recovery (%)
Glucose	197	98.5	198	99	196.5	98.2
L-cysteine	195	97.5	196	98	198	99
L-lysine	194	97	195	97.5	197	98.5
Urea	201	100.5	196	98	198	99
Citric acid	192	96	194	97	196	98
NaCl	196	98	203	101.5	201	100.5
Folic acid	204	102	195	97.5	198	99

Interference amount added = 500 µM; glucose added = 5 mM

During this period, the sensors were stored dry in a refrigerator (4 °C). The DPV peak currents of DA, EP, and NEP remain 91.8%, 92.6%, and 93.4% of the original signals, respectively, showing a slow progressive current decrease. The excellent stability is probably derived from a synergic effect of the nanostructuration and the particular geometry of the microneedle-based electrode, which avoids electrode biofouling. This is a fundamental requirement for a sensor for transdermal continuous analysis.

h-nPG microneedle total catecholamine sensors

The total catecholamine concentration is expressed as NEP concentration, thanks to the best selectivity shown by the NEP sensor, in order to minimize interferences. The influence of the concentration of NEP at the h-nPG microneedle electrode was studied using cyclic voltammetry experiments. CV response for NEP is investigated at various spiked NEP concentrations varying from 1 to 850 μM. The peak current increased with increasing NEP concentration, as shown in Fig. 6. The calibration curve was plotted between the oxidation peak currents (more

visible than cathodic peaks) and NEP concentration, as reported in the inset of Fig. 6 (curve A), displaying a good linearity in the above concentration range. The sensitivity and detection limit were calculated from the plot and found to be 2.4 ± 0.05 μA μM^{-1} cm^{-2} and 0.1 μM at $S/N = 3$, respectively.

Table 2 shows a comparison with the results reported in literature for various nanostructured modified sensors for CA detection. Different nanomaterial-based sensor platforms have been constructed, thanks to the excellent conductivity, biological compatibility, and also enzyme-mimicking ability of the nanomaterials. In particular, three nanoporous modified (no microneedle-based) sensors are reported in the upper part of Table 2. The h-nPG microneedle sensor proposed in this study shows a lower detection limit and a wider linear range compared to the other nanoporous gold no microneedle-based sensors published in literature. Moreover, by comparing the results of the proposed sensor with no microneedle-based sensors modified with different nanomaterials (lower part of Table 2), it is possible to observe a generally wider linear range, with a LOD value higher in some cases [49–52].

Fig. 6 CVs of microneedle h-nPG sensor in 0.1 M PBS, pH = 7.4, and KCl = 0.1 M, at the following NEP concentrations: 0, 5, 10, 20, 30, 50, 60, 75, 100, 185, 450, and 850 μM. Experimental conditions: scan rate = 25 mV s^{-1}; T = 25 °C. In the inset: calibration curve of NEP in phosphate buffer (**A**), in artificial ISF (**B**), and in gel skin model (**C**) (n = 3)
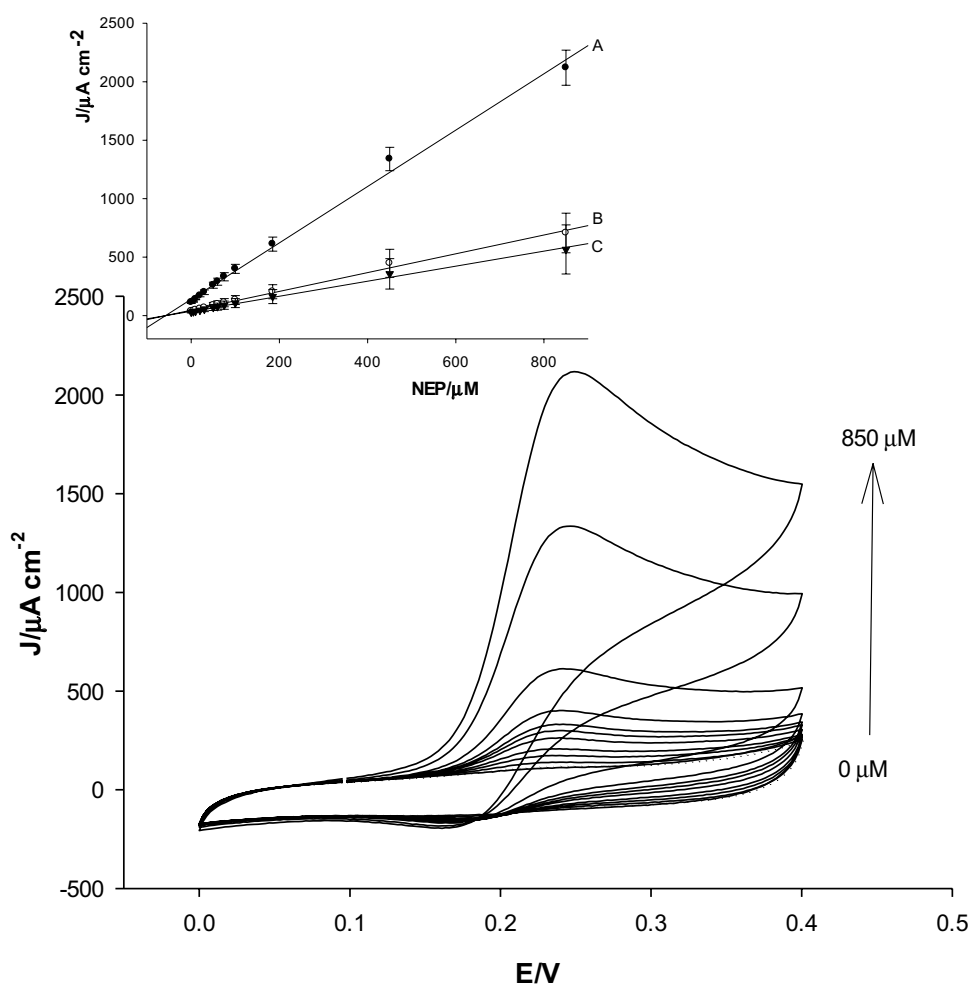
Table 2 Comparison of analytical parameters of nanostructured sensors reported in literature for CA detection

Electrode	Modification strategy	CA	Linear range (μM)	LOD (μM)	Ref
nPG/GCE	Dealloying	DA	-	0.2	[48]
nPG/AuE	Electrodeposition	DA	0.1–40	-	[39]
nPG/AuE	Electrodeposition	EP	50–1000	1.8	[53]
h-nPG/Au microneedles	Electrodeposition	NEP	5–850	0.1	This work
N-UNCD/TiE	Microwave plasma CVD	DA	1–30	-	[59]
ECR/GCE	Electrodeposition	NEP	2–50	1.5	[60]
TiO_2-BH/CPE	Drop casting	NEP	4–1100	0.5	[49]
NMM/CPE	Mixing NMM with graphite powder/ paraffin oil into a paste	NEP	0.07–2000	0.04	[61]
Tyr/CDs/CA/AuE	Cross-linking/physical adsorption	NEP	1–200	0.2	[50]
CeO_2-PEDOT/MWCNT/GCE	Electrodeposition/drop-casting	DA	0.1–10 40–400	0.03	[51]
CNT-Nb	Physical vapor deposition	DA	-	0.011	[52]
RuS_2NPs/GCE	Hydrothermal synthesis	DA	0.1–10	0.074	[54]

In the upper part, nanoporous gold-modified sensors

nPG nanoporous gold, *GCE* glassy carbon electrode, *AuE* gold electrode, *N-UNCD* nitrogen-incorporated ultrananocrystalline diamond, *TiE* titanium electrode, *CVD* chemical vapor deposition, *ECR* eriochrome cyanine, *CPE* carbon paste electrode, *BH = 2,2*-[1, 2] buthanediylbis(nitriloethylidyne)]-bis-hydroquinone, *NMM* nanostructured mesoporous material, *Tyr* tyrosine, *CDs* carbon dots, *CA* cysteamine, *Ce = 2-PEDOT* nanoceria-poly (3,4-ethylenedioxythiophene, *CNT-Nb* carbon nanotube-coated niobium, *RuS₂NPs* ruthenium disulfide nanoparticles

Application of the h-nPG microneedle NEP sensor in artificial ISF and in a gel skin model

Continuous monitoring of CA levels is a significant task in medical diagnostics. Therefore, the analytical performances of the h-nPG microneedle sensor for NEP detection were further assessed in artificial ISF and in a gel skin model, both spiked with NEP. The skin model consists of an agarose (2%) hydrogel opportunely embedded in artificial ISF, in order to mimic the human dermis. The microneedle sensor is immersed into the artificial ISF in the first case and inside the gel in the latter. The calibration curves obtained from the CV responses at different NEP concentrations in artificial ISF and in the skin model are shown in the inset of Fig. 6 (curves B, C). Compared to the results obtained with the same sensor in PBS, the linear ranges are the same, while the sensitivity values slightly lower, resulting $0.80 \pm 0.02 \mu A \mu M^{-1} cm^{-2}$ and $0.64 \pm 0.01 \mu A \mu M^{-1}$ with corresponding LOD values of 0.25 μM and 0.3 μM, for ISF and gel skin model, respectively. This result can be ascribed to the biofouling effect due to protein constituents of the ISF, which causes a slight decrease of the analytical signal.

Conclusions

Herein, we developed the first example of an electrochemical sensing platform for minimally invasive and continuous monitoring of total catecholamine, based on a h-nPG microneedle electrode.

The electroanalytical characterization of the proposed platform indicates the existence of a high electrocatalytic activity in the h-nPG film and its good stability. The self-templated electrochemical deposition resulted to be a fast, reproducible, and eco-friendly technique of electrode modification that avoids the harsh chemicals required for chemical dealloying.

The resulting h-nPG microneedle sensor displays attractive analytical performances for DA, EP, and NEP detection with high sensitivity and selectivity, good reproducibility, and excellent stability. Importantly, it is perfectly biocompatible and allows real-time monitoring of DA, EP, and NEP.

Moreover, the proposed sensor was tested for "in vitro" measurements in artificial ISF and in a gel skin model,

maintaining high sensitivity, a wide linear dynamic range, and high selectivity, compared to PBS.

However, differentiation between the current responses achieved for the three catecholamines was not possible, due to their similar structures giving overlapping oxidation signals.

Future studies will be required to better investigate the correlation between CA concentration in blood and in ISF. It is known that ISF contains similar information to plasma with most small uncharged analytes present at near-equal concentrations in both biofluids, such as glucose and cortisol, as they freely interchange between them by diffusion through the plasma membrane. However, some charged analytes, such as CAs, are commonly found in plasma or in ISF at slightly different concentrations [54], as they cannot traverse the plasma membrane by a simple diffusion process but are shuttled in one of the two compartments [28].

A future goal will be the biouse of the proposed electrochemical platform to develop wearable sensors able to detect CA threshold values to provide diagnostic tools for pathological conditions associated with CA excess (pheochromocytomas and paragangliomas), and thereafter to correlate neurological conditions, such as schizophrenia or Parkinson's to fluctuations in catecholamine levels.

Further efforts will focus on the integration of the microneedle sensor with a wireless electronic interface and wireless transmission for decentralized health status assessment and treatment [55–58].

Although the great potential of the proposed CA sensors in terms of real-time, low cost, high sensitivity, and selectivity, further research and investigations are required along with in vivo studies before practical applications are considered.

Declarations

Conflict of interest The authors declare no competing interests.

References

1. Purves D, Augustine GJ, Fitzpatrick D, Katz LC, LaMantia AS, McNamara JO, Williams SM, Purves D, et al., Eds, Neuroscience, 2nd Edition, Sinauer Associates, Sunderland 2001, 618.

2. Ribeiro JA, Fernandes PMV, Pereira CM, Silva F (2016) Electrochemical sensors and biosensors for determination of catecholamine neurotransmitters: a review. Talanta 160:653–679. https://doi.org/10.1016/j.talanta.2016.06.066

3. Medina MÁ, Urdiales JL, Rodríguez-Caso C, Ramírez FJ, Sánchez-Jiménez F (2003) Biogenic amines and polyamines: similar biochemistry for different physiological missions and biomedical applications. Crit Rev Biochem Mol Biol 38:23–59. https://doi.org/10.1080/713609209

4. Goldstein DS, Mccarty R, Polinsky RJ, Kopin IJ (1983) Relationship between plasma norepinephrine and sympathetic neural activity. Hypertension 5:552–559

5. Marc DT, Ailts JW, Ailts Campeau DC, Bull MJ, Olson KL (2011) Neurotransmitters excreted in the urine as biomarkers of nervous system activity: validity and clinical applicability. Neurosci Biobehav Rev 35:635–644. https://doi.org/10.1016/j.neubiorev.2010.07.007

6. Sbardella E, Maunsell Z, May CJH, Tadman M, James T, Jafar-Mohammadi B, Isidori AM, Grossman AB, Shine B (2020) Random "spot" urinary metanephrines compared with 24-h urinary and plasma results in phaeochromocytomas and paragangliomas. Eur J Endocrinol 183:129–139. https://doi.org/10.1530/eje-19-0809

7. Carrera V, Sabater E, Vilanova E, Sogorb MA (2007) A simple and rapid HPLC–MS method for the simultaneous determination of epinephrine, norepinephrine, dopamine and 5-hydroxytryptamine: application to the secretion of bovine chromaffin cell cultures. J Chromatogr B Anal Technol Biomed Life Sci 847:88–94. https://doi.org/10.1016/j.jchromb.2006.09.032

8. Barreto WJ, Barreto SRG, Ando RA, Santos PS, Di Mauro E, Jorge T (2008) Raman, IR, UV-Vis and EPR characterization of two copper dioxolene complexes derived from L-dopa and dopamine. Spectrochim Acta Part A Mol Biomol Spectrosc 71:1419–1424. https://doi.org/10.1016/j.jneumeth.2004.04.041

9. Syslová K, Rambousek L, Kuzma M, Najmanová V, Bubeníková-Valešová V, Šlamberová R, Kačer P (2011) Monitoring of dopamine and its metabolites in brain microdialysates: method combining freeze-drying with liquid chromatography-tandem mass spectrometry. J Chromatogr A 1218:3382–3391. https://doi.org/10.1016/j.chroma.2011.02.006

10. Wabaidur SM, Alothman ZA, Alam SM, Lee SH (2012) Flow injection–chemiluminescence determination of dopamine using potassium permanganate and formaldehyde system. Spectrochim Acta Part A Mol Biomol Spectrosc 96:221–225. https://doi.org/10.1016/j.talanta.2006.05.078

11. Eddin FBK, Fen YW (2020) Recent advances in electrochemical and optical sensing of dopamine. Sensors 20:1039. https://doi.org/10.3390/s20041039

12. Huffman ML, Venton BJ (2008) Electrochemical properties of different carbon-fiber microelectrodes using fast-scan cyclic voltammetry. Electroanalysis 20:2422–2428. https://doi.org/10.1002/elan.200804343

13. Lane RF, Blaha CD (1990) Detection of catecholamines in brain tissue: surface-modified electrodes enabling in vivo investigations of dopamine function. Langmuir 6:56–65

14. Demuru S, Deligianni H (2017) Surface PEDOT: Nafion coatings for enhanced dopamine, serotonin and adenosine sensing. J Electrochem Soc 164:129–138. https://doi.org/10.1149/2.1461714jes

15. Durairaj S, Sidhureddy B, Cirone J, Chen A (2018) Nanomaterials-based electrochemical sensors for in vitro and in vivo analyses of neurotransmitters. Appl Sci 8:1504. https://doi.org/10.3390/app8091504

16. Dong W, Ren Y, Bai Z, Jiao J, Chen Y, Han B, Chen Q (2018) Synthesis of tetrahexahedral Au-Pd core–shell nanocrystals and reduction of graphene oxide for the electrochemical detection of epinephrine. J Colloid Interface Sci 512:812–818. https://doi.org/10.1016/j.jcis.2017.10.071

17. Schmidt AC, Wang X, Zhu Y, Sombers LA (2013) Carbon nanotube yarn electrodes for enhanced detection of neurotransmitter dynamics in live brain tissue. ACS Nano 7:7864–7873. https://doi.org/10.1021/nn402857u

18. Numan A, Shahid MM, Omar FS, Ramesh K, Ramesh S (2017) Facile fabrication of cobalt oxide nanograin-decorated reduced graphene oxide composite as ultrasensitive platform for dopamine detection. Sens Actuators B Chem 238:1043–1051. https://doi.org/10.1016/j.snb.2016.07.111

19. Lei Y, Butler D, Lucking MC, Zhang F, Xia T, Fujisawa K, Ebrahimi, (2020) Single-atom doping of MoS_2 with manganese enables ultrasensitive detection of dopamine: experimental and computational approach. Science Advances 6: eabc4250. https://doi.org/10.1126/sciadv.abc4250

20. Cheng CF, Hsueh HY, Lai CH, Pan CJ, Hwang BJ, Hu CC, Ho R (2015) Nanoporous gyroid platinum with high catalytic activity from block copolymer templates via electroless plating. NPG Asia Mater 7:e170. https://doi.org/10.1038/am.2015.13

21. Tsujimura S, Murata K, Akatsuka W (2014) Exceptionally high glucose current on a hierarchically structured porous carbon electrode with "wired" flavin adenine dinucleotide dependent glucose dehydrogenase. JACS 136:14432–14437. https://doi.org/10.1021/ja5053736

22. Bollella P, Hibino Y, Kano K, Gorton L, Antiochia R (2018) Highly sensitive membraneless fructose biosensor based on fructose dehydrogenase immobilized onto aryl thiol modified highly porous gold electrode: characterization and application in food samples. Anal Chem 90:12131–12136. https://doi.org/10.1021/acs.analchem.8b03093

23. Sanzó G, Taurino I, Antiochia R, Gorton L, Favero G, Mazzei F, De Micheli G, Carrara S (2016) Bubble electrodeposition of gold porous nanocorals for the enzymatic and non-enzymatic detection of glucose. Bioelectrochemistry 112:125–131. https://doi.org/10.1016/j.bioelechem.2016.02.012

24. Silva TA, Khan Md RK, Fatibello-Filho O, Collinson MM (2019) Simultaneous electrochemical sensing of ascorbic acid and uric acid under biofouling conditions using nanoporous gold electrodes. J Electroanal Chem 846:113160. https://doi.org/10.1016/J.JELECHEM.2019.05.042

25. Lenders JWM, Duh QY, Eisenhofer G, Gimenez-Roqueplo AP, Grebe SKG, Murad MH, Naruse M, Pacak K, Young W (2014) Pheochromocytoma and paraganglioma: an endocrine society clinical practice guideline. J Clin Endocrinol Metab 99:1915–1942. https://doi.org/10.1210/jc.2014-1498

26. Lenders JWM, Pacak K, Walther MM, Linehan WM, Mannelli M, Friberg P, Keiser HR, Goldstein DS, Eisenhofer G (2002) Biochemical diagnosis of pheochromocytoma: which test is best? JAMA 287:1427–1434. https://doi.org/10.1001/jama.287.11.1427

27. Muralidharan R, Chandrashekhar V, Butler D, Ebrahimi A (2020) A smartphone-interfaced, flexible electrochemical biosensor based on graphene ink for selective detection of dopamine. IEE Sensors Journal 20:13204–13211. https://doi.org/10.1109/JSEN.2020.3005171

28. Heikenfeld J, Jajack A, Feldman B, Granger SW, Gaitonde S, Begtrup G, Katchman BA (2019) Accessing analytes in biofluids for peripheral biochemical monitoring. Nature Biotechnol 37:407–419. https://doi.org/10.1038/s41587-019-0040-3

29. Kashaninejad N, Munaz A, Moghadas H, Yadav S, Umer M, Nguyen NT (2021) Microneedle arrays for sampling and sensing skin interstitial fluid. Chemosensors 9:83. https://doi.org/10.3390/chemosensors9040083

30. Tevmourian H, Tehrani F, Mahato K, Wang J (2021) Lab under the skin: microneedles based wearable devices. Adv Healthcare Mat 10 https://doi.org/10.1002/adhm.202002255

31. Bollella P, Sharma S, Cass AEG, Antiochia R (2019) Microneedle-based biosensor for minimally-invasive lactate detection. Biosens Bioelectron 123:152–159. https://doi.org/10.1016/j.bios.2018.08.010

32. Cass AEG, Sharma S (2017) Microneedle enzyme sensor arrays for continuous in vivo monitoring. Methods Enzymol 589:413–427. https://doi.org/10.1016/bs.mie.2017.02.002

33. Tasca F, Tortolini C, Bollella P, Antiochia R (2019) Microneedle-based electrochemical devices for transdermal biosensing: a review. Curr Opin Electrochem 16:42–49. https://doi.org/10.1016/j.coelec.2019.04.003

34. Goud KY, Moonla C, Mishra RK, Yu C, Narayan R, Litvan I, Wang J (2019) Wearable electrochemical microneedle sensor for continuous monitoring of levodopa: toward Parkinson management. ACS Sens 4:2196–2204. https://doi.org/10.1021/acssensors.9b01127

35. Saito N, Adachi H, Tanaka H, Nakata S, Kawada N, Oofusa K, Yoshizato K (2017) Interstitial fluid flow-induced growth potential and hyaluronan synthesis of fibroblasts in a fibroblast-populated stretched collagen gel culture. Biochim Biophys Acta Gen Subj 1861:2261–2273. https://doi.org/10.1016/j.bbagen.2017.06.019

36. Bollella P, Sharma S, Cass AEG, Tasca F, Antiochia R (2019) Minimally invasive glucose monitoring using a highly porous gold microneedles-based biosensor: characterization and application in artificial interstitial fluid. Catalysts 9:580. https://doi.org/10.3390/catal9070580

37. Randviir EP (2018) A cross examination of electron transfer rate constants for carbon screen-printed electrodes using Electrochemical Impedance Spectroscopy and cyclic voltammetry. Electrochim Acta 186:179–186. https://doi.org/10.1016/j.electacta.2018.08.021

38. Bard AJ, Faulkner LR (2001) Electrochemical methods fundamentals and applications. Wiley, New York

39. Said WE, Lee JH, Oh BK, Choi JW (2010) 3-D nanoporous gold thin film for the simultaneous electrochemical determination of dopamine and ascorbic acid. Electrochem Comm 12:1756–1759. https://doi.org/10.1016/j.elecom.2010.10.015

40. Lavagnini I, Antiochia R, Magno F (2004) An extended method for the practical evaluation of the standard rate constant from cyclic voltammetric data. Electroanal 16:505–506

41. Lavagnini I, Antiochia R, Magno F (2007) A calibration-based method for the evaluation of the detection limit of an electrochemical biosensor. Electroanal 19:1227–1230

42. Patel AN, Tan S, Miller TS, Macpherson JV, Unwin P (2016) Comparison and reappraisal of carbon electrodes for the voltammetric detection of dopamine. Anal Chem 85:11755–11764. https://doi.org/10.1021/ac401969q

43. Sainz R, del Pozo M, Vilas-Varela M, Castro-Esteban CMP, Vázquez L, Blanco E, Martin-Gago JA, Ellis GJ, Petit-Dominiguez MD, Quintana C, Casero E (2020) Chemically synthesized chevron-like graphene nanoribbons for electrochemical sensors development: determination of epinephrine. Sci Rep 10:14614. https://doi.org/10.1038/s41598-020-71554-1

44. Arulraj AD, Arunkumar A, Vijayan M, Viswanath KB, Vasantha VS (2016) A simple route to develop highly porous nano polypyrrole/reduced graphene oxide composite film for selective

determination of dopamine. Electrochim Acta 206:77–85. https://doi.org/10.1016/j.electacta.2016.04.134

45. Laviron EJ (1979) General expression of the linear potential sweep voltammogram in the case of diffusionless electrochemical systems. Electroanal Chem 101:19–28. https://doi.org/10.1016/S0022-0728(79)80075-3

46. Mphuthi NG, Adekunle AS, Ebenso EE (2016) Electrocatalytic oxidation of epinephrine and norepinephrine at metal oxide doped phthalocyanine/MWCNT composite sensor. Scientific Rep 6:26938. https://doi.org/10.1038/srep26938

47. Gao F, Cai X, Wang X, Gao C, Liu S, Gao F, Wang Q (2013) Highly sensitive and selective detection of dopamine in the presence of ascorbic acid at graphene oxide modified electrode. Sens Act B 186:380–387. https://doi.org/10.1016/j.snb.2013.06.020

48. Qiu HJ, Zhou GP, Ji GL, Zhang Y, Huang XR, Ding Y (2008) A novel nanoporous gold modified electrode for the selective determination of dopamine in the presence of ascorbic acid. Coll Surf B Biointerfaces 69:105–108. https://doi.org/10.1016/j.colsurfb.2008.11.007

49. Ardakani MM, Beitollahi H, Sheikh-Mohseni MA, Naeimi H, Taghavinia N (2010) Novel nanostructure electrochemical sensor for electrocatalytic determination of norepinephrine in the presence of high concentrations of acetaminophene and folic acid. Appl Catal A 378: 195–201. https://www.cheric.org/research/tech/periodicals/doi.php?art_seq=844063

50. Baluta S, Lesiak A, Cabaj J (2020) Simple and cost-effective electrochemical method for norepinephrine determination based on carbon dots and tyrosinase. Sensors 20:4567. https://doi.org/10.3390/s20164567

51. Üge A, Zeybek DK, Zeybek B (2018) An electrochemical sensor for sensitive detection of dopamine based on MWCNTs/CeO$_2$-PEDOT composite. J Electroanal Chem 15:134–142. https://doi.org/10.1016/j.jelechem.2018.02.028

52. Yang C, Jacobs CB, Nguyen MD, Ganesana M, Zestos AG, Ivanov IN, Puretzky AA, Rouleau CM, Geohegan DB, Venton BJ (2016) Carbon nanotubes grown on metal microelectrodes for the detection of dopamine. Anal Chem 88:645–652. https://doi.org/10.1021/acs.analchem.5b01257

53. Fouad DM, Said WA (2016) Selective electrochemical detection of epinephrine using gold nanoporous film. Journal of Nanomaterials 6194230. https://doi.org/10.1155/2016/6194230

54. Deepika J, Sha R, Badhulika S (2019) A ruthenium(IV) disulfide based non-enzymatic sensor for selective and sensitive amperometric determination of dopamine. Microchim Acta 186:480. https://doi.org/10.1007/s00604-019-3622-3

55. Samant PP, Niedzwiecki MM, Raviele N, Tran V, Lapaix JM, Walker DI, Felner EI (2020) Sampling interstitial fluid from human skin using a microneedle patch. Sci Translat Med 12:0285. https://doi.org/10.1126/scitranslmed.aaw0285

56. Ferreira PC, Ataíde VN, Silva Chagas CL, Angnes L, Tomazelli Coltro WK, Paixão LG, Reis de Araujo W (2019) Wearable electrochemical sensors for forensic and clinical applications. Trends Anal Chem 119:115622. https://doi.org/10.1016/j.trac.2019.115622

57. Garcia Guzman JG, Perrez Rafols C, Gaston MC, Crespo A (2021) Microneedle based electrochemical (Bio)Sensing: towards decentralized and continuous health status monitoring. TrAC 135:116148. https://doi.org/10.1016/j.trac.2020.116148

58. Kim J, Campbell AS, Fernández de Avila BE, Wang J (2019) Wearable biosensors for healthcare monitoring. Nat Biotechnol 37:389–406. https://doi.org/10.1038/s41587-019-0045-y

59. Skoog SA, Miller PR, Boehm RD, Sumant AV, Polsky R, Narayan RJ (2015) Nitrogen-incorporated ultrananocrystalline diamond microneedle arrays for electrochemical biosensing. Diam Relat Mater 54:39–46. https://doi.org/10.1016/j.diamond.2014.11.016

60. Yao H, Li S, Tang Y, Chen Y, Chen Y, Lin X (2009) Selective oxidation of serotonin and norepinephrine over eriochrome cyanine R film modified glassy carbon electrode. Electrochim Acta 54:4607–4612. https://doi.org/10.1016/j.electacta.2009.02.108

61. Ardakani MM, Mohseni MA, Alibeik MA, Benvidi A (2012) Electrochemical sensor for simultaneous determination of norepinephrine, paracetamol and folic acid by a nanostructured mesoporous material. Sens Actuators B 171–172:380–386. https://doi.org/10.1016/j.snb.2012.04.071